# Dynamics of magnetic microswimmers

Author: Mariona Cortés Marimon, mcortema15@alumnes.ub.edu
*Facultat de Física, Universitat de Barcelona, Diagonal 645, 08028 Barcelona, Spain.*

Advisor: Helena Massana-Cid and Pietro Tierno

**Abstract:** This work explores the dynamics of magnetic microswimmers composed of anisotropic hematite particles driven by external magnetic fields. We first measured the magnetic moment of ellipsoidal and peanut-shaped colloids by analyzing their reorientation under a static magnetic field. We then focused on achieving propulsion by applying a rotating field to the peanut-shaped particles and studying their motion near a solid-liquid interface. Specifically, we measured their average speed as a function of the field's driving frequency during propulsion. We found two dynamic states separated by a critical frequency: a synchronous regime where colloids display increasing speed with frequency, and an asynchronous regime, where viscous drag dominates and speed decreases. The values of the critical frequencies were extracted from the experimental data for different field amplitudes. The results align with the theoretical model and show a form of non-reciprocal motion leading to propulsion in the low Reynolds number regime.

**Keywords:** Magnetic microswimmers, propulsion at low Reynolds numbers, magnetic colloids
**SDGs:** Quality education.

## I. INTRODUCTION

Self-propelled systems at the microscale have become increasingly relevant due to their wide range of applications in diverse fields such as microfluidics [1], drug delivery [2], biomedicine [3] or transport of small cargoes [4]. Currently, there are multiple approaches to designing better, faster and more environmentally adaptable microswimmers. These strategies not only serve technological applications, but also help deepen our understanding of the fundamental physics that govern their dynamics in viscous fluids [5]. One of the main challenges in designing entities capable of propulsion in the microsale is the fact that, at the low Reynolds number regime, viscous forces dominate over inertial ones. As a consequence, the Navier-Stokes equations become time-reversible, and any reciprocal motion, i.e. any sequence of displacements or body deformations that are identical when reversed in time, will not induce a net motion [6]. This condition alters traditional approaches, such as those used for macroscopic systems, and complicates the development of effective propulsion mechanisms at the microscale. Magnetic colloids - systems where microscopic magnetic particles are dispersed in a liquid medium - offer a highly promising approach in this field [7]. These particles allow for precise and remote control through external magnetic fields [8]. Since they do not require an internal power source, their energy consumption is minimal. Moreover, unlike electric fields, magnetic fields do not alter the dispersing medium. One effective strategy involves applying a rotating magnetic field which, in the presence of a surface, enables magnetic colloids to perform rolling motion. This process is non-reciprocal, producing net propulsion at the low Reynolds number regime. In this work, we experimentally studied the dynamics of micrometric anisotropic hematite particles. These particles are ferromagnetic, meaning they possess a permanent magnetic moment, which in this case is aligned along their short axis. Due to their shape anisotropy, the orientation of the magnetic moment can be inferred when observing the particles under a microscope. This work investigates the individual dynamics of colloids dispersed in water under the influence of magnetic fields: first we focused on determining the particles' magnetic moment. For this purpose, we applied a static magnetic field and tracked the corresponding reorientation of the particles (Section IV A). Measuring the particles' magnetic moment is crucial to determine the particle-field coupling strength. The second part of this study explores how to achieve propulsion by applying a rotating magnetic field perpendicular to the sample's plane (Section IV B). This field induces a torque on the magnetic particles, causing them to rotate. Since the particles are located near a surface, their rotation generates a flow that is altered by the solid boundary, which enforces no-slip boundary conditions. In the low Reynolds number regime, surface proximity breaks the symmetry of the flow field, resulting in a net propulsion of the colloids [6]. The aim of this section is to analyze the dependence of the propulsion velocity on the frequency of the applied field.

## II. EXPERIMENTAL METHODOLOGY

The hematite particles used in this study were synthesized by Dezhou Cao and Helena Massana-Cid using the sol-gel method, which enables the production of monodisperse particles with various shapes [8, 9]. In this work, we have studied two types of colloids of different shapes and sizes: ellipsoidal particles with axes $a = (2.14 \pm 0.02)$ $\mu$m and $b = (1.513 \pm 0.016)$ $\mu$m, and peanut-shaped particles with axes $a = (2.97 \pm 0.07)$ $\mu$m and $b = (1.76 \pm 0.04)$ $\mu$m. The dimensions were determined using scanning electron microscope (SEM) images (Fig 1). As the original solu-

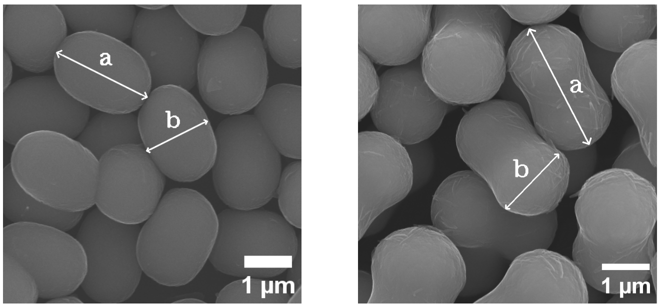


(a) Ellipsoidal particles (b) Peanut-shaped particles

FIG. 1: Scanning electron microscope images of the ellipsoidal and peanut-shaped particles used in this study.

tion had a high particle density, the following protocol was used to dilute the particles and avoid aggregation. First, we mixed 10 mL of distilled water with 10 $\mu$L of Tween 20, a surfactant that prevented particle aggregation and improved their dispersion. Next, we took 1 mL of this solution and added 0.5 $\mu$L of the original particle solution. We then introduced this final solution into a capillary tube of inner dimensions $0.1-2$ mm (CMC Scientific) and sealed it with candle wax to observe the particles under the microscope. The density difference between hematite and water caused the particles to sediment near the base of the capillary, forming a confined monolayer. This quasi-two-dimensional confinement was an essential condition to obtain a stable visualization of the particle dynamics.

The sample was then placed under a light microscope, specifically a Nikon Eclipse Ni, equipped with a charge-coupled device (CCD) camera. This setup allowed us to record videos of the particles' motion and observe them in real time through a computer interface. The objectives used had two different magnification levels (denoted with $\times$) and numerical aperture (NA): 100$\times$ with 1.30 NA and 40$\times$ with 0.60 NA (Nikon). The choice of the objective depended on the resolution required for each observation. Videos were recorded at 75 fps and 25 fps.

To apply external magnetic fields, a set of Helmholtz coils was connected to a waveform generator (TGA1244, TTi) feeding a poweramplifier (AMP-1800) and a direct current power supply (EL 302RT, TTi). The coil configuration consisted of two coils along the $x$-direction, two along the $y$-direction and one coil placed beneath the sample, representing the $z$-direction, where (x,y) represented the sample's plane and $z$ the perpendicular direction. This arrangement enabled the generation of a uniform magnetic field in all three spatial directions. For particle tracking and data analysis, a custom Python program was developed. This program incorporated OpenCV for image processing and Matplotlib for visualization. This approach allowed the determination of the particles' positions and the reconstruction of their trajectories.

## III. PARTICLE DYNAMICS

In the first set of experiments (Section IV A), the objective was to measure the magnitude of the magnetic moment $m$. The application of an external static field leads to a reorientation of the particles, which align their magnetic moment along the direction of the field [10]. The dependence of the reorientation dynamics on $m$ allowed for its quantitative determination through the following procedure. First a magnetic field along the $y$-direction was applied to set an initial orientation for all the particles. This field was then turned off, and a new static field was applied along the perpendicular direction ($x$-direction). This procedure ensures that the angle $\theta$ between the particles' major axis and the $x$-axis during the reorientation spans from 0° to 90°, as shown in Fig. 2. One can describe the reorientation

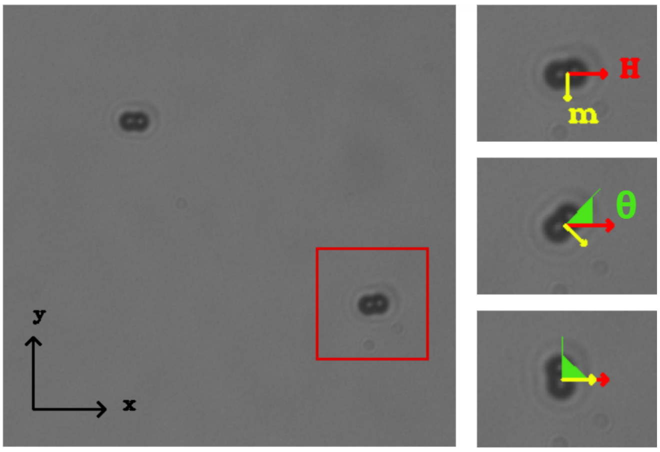


FIG. 2: Microscope image showing two peanut-shaped particles aligned along the initial field direction (left). Images showing a particle's reorientation under a magnetic field applied in the $x$-direction (right). Times increase from top to bottom. The yellow arrow denotes the magnetic moment $\boldsymbol{m}$, the red arrow the field $\boldsymbol{H}$ and the green region the angle $\theta$.

dynamics of the hematite particles by considering the balance between the external magnetic torque ($\boldsymbol{\tau}_m$) and the viscous one arising from the rotation in water ($\boldsymbol{\tau}_v$). The first torque is given by the vector product between the magnetic moment ($\boldsymbol{m}$) and the magnetic field ($\boldsymbol{H}$): $\boldsymbol{\tau}_m = \mu_w \boldsymbol{m} \times \boldsymbol{H}$, being $\mu_w = 4 \cdot 10^{-7}$ H/m the magnetic permeability of the water [10]. Since the particles rotate in the fluid, they experience a viscous torque that opposes this motion: $\boldsymbol{\tau}_v = -\xi_r \dot{\boldsymbol{\theta}}$, where $\theta$ is the particles' orientation angle with respect to the $x$-axis and $\xi_r$ is the rotational friction coefficient of the particles. This quantity is defined as $\xi_r = 8\pi\eta V_c f_r$, where $V_c$ is the volume of the particles, $f_r$ is a geometrical factor that depends on the particles' shape [10] and $\eta = 10^{-3}$ Pa $\cdot$ s is the dynamic viscosity of the water. At low Reynolds numbers, inertia is negligible, and the system rapidly reaches mechanical equilibrium. Thus, the torque balance is given by:

$$\boldsymbol{\tau_m} + \boldsymbol{\tau_v} = 0 \ . \tag{1}$$

By solving the above equation, one can obtain an expression for how the orientation angle evolves over time [10]:

$$\theta(t) = 2\tan^{-1}\left[\tanh\left(\frac{t}{\tau_r}\right)\right] \ . \tag{2}$$

Here, $\tau_r$ is the relaxation time which characterizes the timescale over which the particles reorient in response to a magnetic field. It is given by:

$$\tau_r = \frac{2\xi_r}{\mu_w m H} \ . \tag{3}$$

By measuring $\tau_r$, we can determine the magnetic moment using Eq. (3).

The aim of the second series of experiments (Section IV B) is to achieve propulsion of the magnetic colloids. To this end, a rotating magnetic field is applied in the perpendicular plane of the sample (x,z) described by $H(t) = H[\cos(2\pi f t)\hat{x} - \sin(2\pi f t)\hat{z}]$, where $H$ is the field amplitude and $f$ the driving frequency. When the rotating magnetic field is applied, the magnetic colloids experience a torque that induces rotation along the $y$-axis. In a bulk fluid, this rotation would generate a vortical, symmetric flow around the particles, resulting in no net displacement. However, near a liquid-solid interface (represented by the capillary wall), the fluid must satisfy the no-slip boundary condition. This constraint alters the flow generated by the rotating particles, breaking the time-reversal symmetry of the fluid. As a consequence, a net propulsion emerges, oriented perpendicular to the rotation axis ($y$-axis). Since the particles are confined within the capillary, the resulting propulsion occurs along the $x$-direction [11], as illustrated in the trajectories overlaid to the microscope image in Fig. 3 and the displacement reported in Fig. 4.

The resulting transport of the particles exhibits two distinct regimes separated by a critical frequency $f_c$. For frequencies below $f_c$ , the particles rotate in phase with the applied field (synchronous regime). This results in a linear increase in the propulsion velocity, which can be described as $v_x = 2\pi a\gamma f$, where $a$ is the particles' long axis and $\gamma$ is a prefactor related to wall effects [12].
Beyond $f_c$, viscous drag increases and prevents the particles from fully synchronizing with the field (asynchronous regime). This leads to a decrease in the average propulsion velocity given by the relation $\langle v_x\rangle = 2\pi a\gamma(f - \sqrt{f^2 - f_c^2})$ [12]. Thus, the particle average velocity can be expressed as:

$$\langle v_x\rangle = \begin{cases} 2\pi a\gamma f & \text{if } f < f_c \\ 2\pi a\gamma(f - \sqrt{f^2 - f_c^2}) & \text{if } f > f_c \end{cases} \tag{4}$$

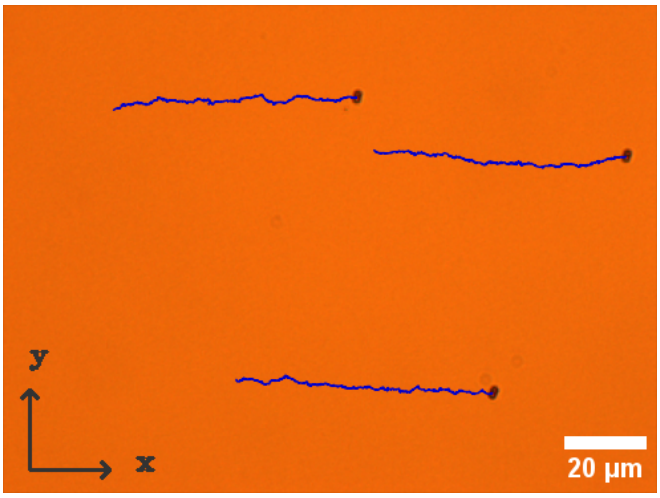


FIG. 3: Trajectories of the peanut-shaped colloids when subjected to a rotating field in the $(x,z)$ plane of amplitude $H = 398$ A/m and frequency $f = 20$ Hz.

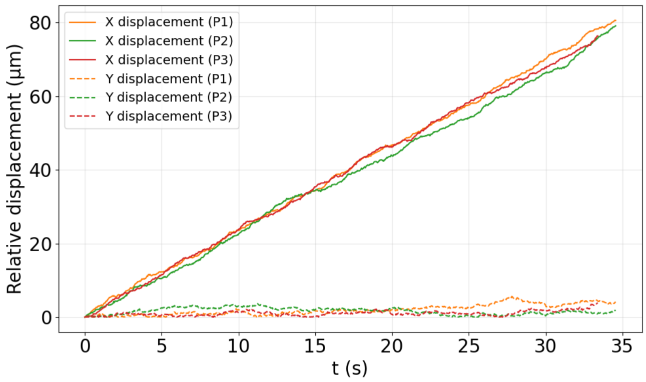


FIG. 4: Time evolution of relative displacement along the $X$ (solid lines) and $Y$ (dashed lines) directions for three individual particles (P1, P2, and P3). The colloids are subjected to a magnetic field of amplitude $H = 398$ A/m and driving frequency of $f = 20$ Hz.

## IV. RESULTS

### A. Measurement of the magnetic moment

This subsection presents the results obtained from the study of the temporal evolution of the particles' orientation under a static magnetic field applied along the $x$-direction with an amplitude of $H = 955$ A/m. The analysis focused on the reorientation dynamics of both ellipsoidal and peanut-shaped particles.
In order to determine the magnitude of the magnetic moment, we recorded the evolution of the orientation angle $\theta(t)$ as a function of time. The experimental data were then fitted to Eq. (2) to determine the relaxation time $\tau_r$. Using the obtained $\tau_r$ combined with the values of the other parameters in Eq. (3), the magnetic moment

$m$ was calculated. The time evolution of the orientation angle for peanut-shaped particles under the influence of the applied field is shown in Fig. 5. The particles reach their aligned state in a relaxation time of $\tau_r = (0.033 \pm 0.004)$ s. Using this value and Eq.(3), we determined the strength of the particles' magnetic moment to be: $m = (8.8 \pm 1.1) \cdot 10^{-16}$ Am$^2$. Fig. 6 presents the orientation angle of ellipsoidal particles under the same magnetic field. In this case, the obatined relaxation time is $\tau_r = (0.089 \pm 0.006)$ s, and the magnetic moment is $m = (21.1 \pm 1.4) \cdot 10^{-17}$ Am$^2$.

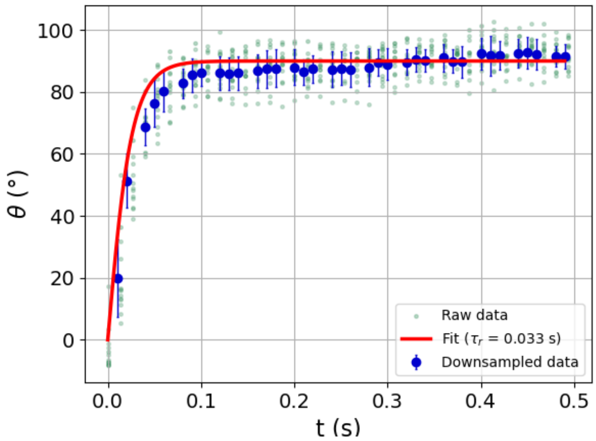


FIG. 5: Time evolution of the angle $\theta$ for peanut-shaped particles under a field applied along the $x$-direction with amplitude $H = 955$ A/m. Green dots represent raw data, blue circles denote averaged values and the continuous line is a fit to determine $\tau_r$. $t = 0$ s corresponds to the instant when the magnetic field in the $x$-direction is applied.

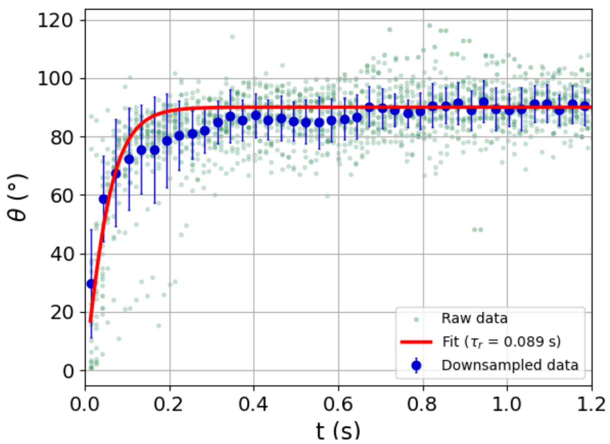


FIG. 6: Time-dependent orientation of the ellipsoidal particles under an external magnetic field of amplitude $H = 955$ A/m. Green dots represent raw data, blue circles denote averaged data and the continuous line is a fit to determine $\tau_r$.

Although the averaged curves allow for a precise estimation of $\tau_r$, both figures reveal a noticeable dispersion in the raw data. This variability likely arises from intrinsic differences between particles in size, shape, or hematite content, which affect their magnetic response.

The determined values are consistent with those reported in previous studies, such as in Ref. [10]. The small differences observed may be attributed to the fact that these particles were synthesized via different chemical procedures and may present varying concentrations of the magnetic material.

### B. Microparticles' propulsion

The aim of this subsection is to characterize how the propulsion velocity of individual particles, achieved as described in the previous section, depends on the driving frequency of the field.

This part of the study focused exclusively on peanut-shaped colloids, as the ellipsoidal particles used possessed relatively smaller magnetic moments and required stronger fields to be propelled in water. In particular, we characterized their average speed by varying $f$ at three distinct field amplitudes: $H_1 = 398$ A/m, $H_2 = 1114$ A/m and $H_3 = 2387$ A/m. This approach allowed us to fit the experimental data to the velocity equations (Eq. (4)) for both regimes and determine the corresponding critical frequency. Fig. 7 shows how the mean velocity in the $x$-direction ($\langle v_x \rangle$) depends on the driving frequency ($f$) for each tested magnetic field amplitude. In the synchronous regime ($f < f_c$), the colloids rotate synchronously with the field, resulting in a linear increase of $\langle v_x \rangle$ with the frequency. This behavior is consistent with theoretical expectations at low frequencies, where magnetic torque dominates over viscous drag. As the frequency increases beyond the critical frequency, the system enters the asynchronous regime. In this regime, the particles are no longer able to follow the rotation of the field due to the increasing dominance of viscous forces. This leads to a non-linear decrease in $\langle v_x \rangle$, indicating the loss of synchronization with the rotating field. Note that increasing the field amplitude raises the maximum value of $\langle v_x \rangle$ by up to a factor 5.

We identify the critical frequency as the intersection point of the linear and non-linear fits. For the amplitude $H = 1114$ A/m the two fits intersect clearly. The critical frequency was determined to be $f_c = 74.2$ Hz. For the amplitudes $H = 398$ A/m and $H = 2387$ A/m (first and third panels in Fig. 7), there is a lower agreement between the predicted behavior in the transition regime and the experimental data. This deviation could be attributed to the presence of dispersion on the particles' magnetic moment, shown in Fig. 5. Different magnetic moments may induce a dispersion in the particles' velocity near

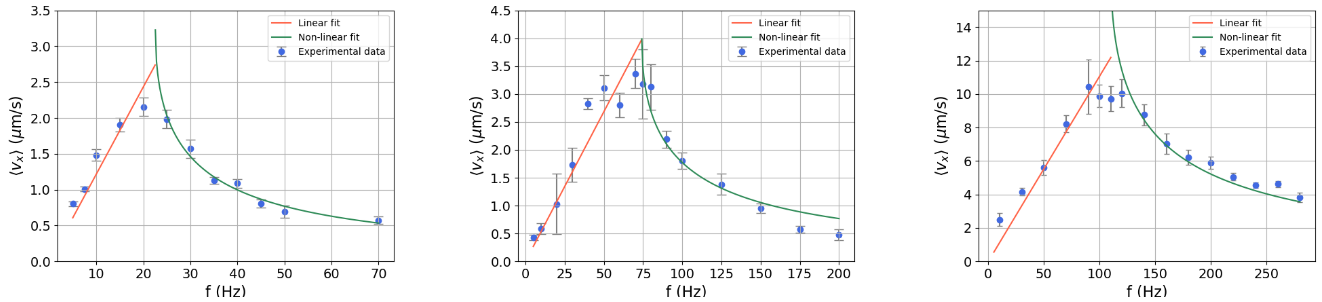


(a) Amplitude: $H = 398$ A/m; $f_c = 22.6$ Hz.

(b) Amplitude: $H = 1114$ A/m; $f_c = 74.2$ Hz.

(c) Amplitude: $H = 2387$ A/m; $f_c = 110.2$ Hz.

FIG. 7: Dependence of the mean velocity component along the $x$ axis $\langle v_x \rangle$ on the driving frequency $f$ for various magnetic field amplitudes $H$.

the critical frequency when applying a rotating magnetic field. To improve the reliability of the fits, a larger experimental dataset around the critical region would be necessary. Despite these uncertainties, we estimated the critical frequency by finding the value that minimized the error of the fit. The obtained values are shown in Table I.

| Field amplitude, $H$ (A/m) | Critical frequency, $f_c$ (Hz) |
|---|---|
| 398 | 22.6 |
| 1114 | 74.2 |
| 2387 | 110.2 |

TABLE I: Values of the determined critical frequencies ($f_c$) for peanut-shaped colloids under different magnetic field amplitudes ($H$).

## V. CONCLUSIONS

This work focused on investigating the non-equilibrium dynamics of magnetic microswimmers at low Reynolds numbers driven by external magnetic fields. First, the magnetic moments of anisotropic hematite particles (peanut-shaped and ellipsoidal) were determined by analyzing their reorientation under a static field. The results show that peanut-shaped particles exhibit a stronger magnetic moment compared to ellipsoidal colloids, consistent with their larger volume. Additionally, ellipsoidal particles have a greater dispersion in their magnetic moment, which could be attributed to their chemical synthesis. Second, we achieved directed motion of the peanut-shaped particles by applying a rotating magnetic field. As shown in Table I, the critical frequency $f_c$ increases with the magnetic field amplitude. These findings confirm that non-reciprocal motion of these magnetic miscroswimmers is possible near solid-liquid interfaces, enabling propulsion at low Reynolds numbers.

**Acknowledgments**

I would like to thank my advisor, Pietro Tierno, for his trust and for giving me the opportunity to learn and develop this project. I would also like to express my deepest gratitude to Helena Massana-Cid for her invaluable guidance and continuous support throughout this work. I have learned a lot from both of them, and this project would not have been possible without their contributions.

[1] J. Liu *et al. Appl. Mater. Today*, **25**, 101327 (2021)
[2] M. Luo, Y. Feng, T. Wang and J. Guan, *Adv. Funct. Mater.*, **28**, 1706100 (2018).
[3] B. J. Nelson, I. K. Kaliakatsos and J. J. Abbott, *Annu. Rev. biomed. Eng.* **12** 55-85 (2010).
[4] Y. Alapan, O. Yasa, O. Schauer, J. Giltinan, A. F. Tabak, V. Sourjik, and M. Sitti. *Sci. Robot.* **3**, eaar4423 (2018).
[5] J. Katuri, X. Ma, M. M. Stanton, and S. Sánchez. *Acc. Chem. Res.* **50**, 2, 271-279 (2017).
[6] E. M. Purcell. *Am. J. Phys.* **45**, 3 (1977).
[7] X. Z. Chen, C. Xu, H. Ran, L. Zhang, and B. J. Nelson. *Appl. Mater. Today*, **9**, 37–48 (2017).
[8] H. Massana-Cid. **Out-of-equilibrium dynamics in driven and active magnetic colloids**. PhD thesis, Universitat de Barcelona (2019).
[9] T. Sugimoto, M. M. Khan, and A. Muramatsu. *Colloids Surf. A*, **70**, 167–169 (1993).
[10] F. Martinez-Pedrero, A. Cebers, and P. Tierno. *Soft Matter*, **12**, 3688–3695 (2016).
[11] F. Martinez-Pedrero, A. Ortin-Ambriz, I. Pagonabarraga, and P. Tierno, *Phys. Rev. Lett.*, **115**, 138301 (2015).
[12] G. Junot, A. Cebers, and P. Tierno. *Soft Matter*, **17**, 8605–8611 (2021).

# Dinàmica de micronedadors magnètics

Author: Mariona Cortés Marimon, mcortema15@alumnes.ub.edu
*Facultat de Física, Universitat de Barcelona, Diagonal 645, 08028 Barcelona, Spain.*

Advisor: Helena Massana-Cid and Pietro Tierno

**Resum:** Aquest treball investiga la dinàmica de micronedadors magnètics formats per partícules anisotròpiques d'hematita subjectes a camps magnètics externs. Primer, hem mesurat el moment magnètic de col·loides amb morfologia el·lipsoïdal i de cacauet analitzant la seva reorientació sota un camp magnètic estàtic. A continuació, ens hem centrat en aconseguir propulsió aplicant un camp rotatori a les partícules en forma de cacauet i hem estudiat el seu moviment prop d'una interfície sòlid-líquid. En concret, hem mesurat la seva velocitat mitjana en funció de la freqüència del camp aplicat. Hem identificat dos estats dinàmics separats per una freqüència crítica: un règim sincrònic en què els col·loides presenten un augment lineal de la velocitat amb la freqüència, i un règim asincrònic, on la fricció viscosa domina i la velocitat disminueix. Els valors de les freqüències crítiques han estat determinats a partir de les dades experimentals per a diferents amplituds del camp. Els resultats s'ajusten al model teòric i evidencien una forma de moviment no recíproc que condueix a la propulsió en el règim de baix nombre de Reynolds.
**Paraules clau:** Micronedadors magnètics, propulsió a baix nombre de Reynolds, col·loides magnètics.
**ODSs:** Educació de qualitat

**Objectius de Desenvolupament Sostenible (ODSs o SDGs)**

| | | | |
|---|---|---|---|
| 1. Fi de la es desigualtats | | 10. Reducció de les desigualtats | |
| 2. Fam zero | | 11. Ciutats i comunitats sostenibles | |
| 3. Salut i benestar | | 12. Consum i producció responsables | |
| 4. Educació de qualitat | X | 13. Acció climàtica | |
| 5. Igualtat de gènere | | 14. Vida submarina | |
| 6. Aigua neta i sanejament | | 15. Vida terrestre | |
| 7. Energia neta i sostenible | | 16. Pau, justícia i institucions sòlides | |
| 8. Treball digne i creixement econòmic | | 17. Aliança pels objectius | |
| 9. Indústria, innovació, infraestructures | | | |